Spectrochimica Acta Part A: Molecular and Biomolecular Spectroscopy 254 (2021) 119634

Contents lists available at ScienceDirect

Spectrochimica Acta Part A: Molecular and Biomolecular Spectroscopy

journal homepage: www.elsevier.com/locate/saa

Potential liquid crystal-based biosensor depending on the interaction between liquid crystals and proteins

Priyanki Kalita [a], Shashank Sekhar Shukla [b], Ranjan K. Singh [b], Ayon Bhattacharjee [a,*]

[a] Department of Physics, National Institute of Technology, Shillong-793003, Meghalaya, India
[b] Department of Physics, Banaras Hindu University, Varanasi-221005, Uttar Pradesh, India

HIGHLIGHTS

- Liquid crystal-based biosensors uses the birefringent properties of liquid crystal (LC) molecules under a polarising optical microscope.
- The change in orientational ordering of the molecules takes place in the presence of Human serum albumin (HSA).
- The LC 4′-pentyl-4-biphenylcarbonitrile (5CB) acts as a transducing element for converting biological and chemical phenomena into optical signals.
- Molecular docking studies confirms the binding location of 5CB with HSA possessing binding energy of −8.10 kcal/mol.
- The residues of HSA binds with 5CB LC through π-π and hydrophobic interactions.
- Raman spectroscopy confirms the interaction and the vibrational properties on interaction between the 5CB and HSA.

GRAPHICAL ABSTRACT

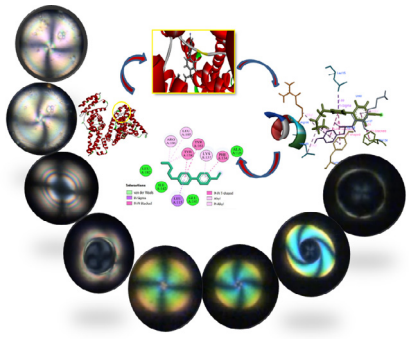

ARTICLE INFO

Article history:
Received 10 December 2020
Received in revised form 3 February 2021
Accepted 15 February 2021
Available online 3 March 2021

Keywords:
Liquid crystal 5CB
Protein human serum albumin
Raman spectra
polarizing optical microscopy (POM)
Molecular docking
Configuration
Alignment

ABSTRACT

Liquid crystal biosensors serve an essential role to detect biomolecules and chemical events as an effective, simple and early detection tool. The detection of Human serum albumin protein by a room temperature liquid crystal 4́-pentyl-4-biphenylcarbonitrile has been investigated using multiple techniques such as Polarizing optical microscope, Raman spectroscopy and molecular docking. The dynamics of director transfigurations of the liquid crystal molecule in the presence of protein through interactions are reported in the study. The change in the alignment of liquid crystal molecules during the nematic phase is observed under a polarizing optical microscope. The interactions through which the liquid crystal molecules bind with protein is depicted from the docking analysis. The residues in the active sites confirm their presence from docking studies. The spectral behaviour has been investigated by temperature-dependent Raman spectroscopy. The findings from Raman spectra for the interaction between these compounds correlates with the residues confirmed from molecular docking analysis.

* Corresponding author.
E-mail address: ayonbh@nitm.ac.in (A. Bhattacharjee).

https://doi.org/10.1016/j.saa.2021.119634
1386-1425/

1. Introduction

Liquid crystals (LCs) are compounds which possess the properties of both liquids and crystalline solids. LCs can flow like a liquid and at the same time, maintain crystal-like order. The order, as well as the orientation, are temperature-dependent. The LC molecules are, in general, oriented in a particular direction indicated by a director [1]. Amongst different LC phases, nematics are generally thermotropic, have a thread-like texture and, have long-range orientational ordering and, no positional ordering. LC-based biosensing uses the birefringence properties of the LC phases, i.e., optical anisotropy of the LC molecules. Due to the anisotropy of LCs, they find wide applications in display devices [2], smart optic devices [3], sensing devices [4,5] and other technological applications. The sensitivity of LCs is used to amplify the presence of some biological species such as proteins [6-9], lipids [10,11] at the LC aqueous interface in terms of optical signals. Therefore, liquid crystals can be used both as sensing and transducing element in biosensors [6,12,13]. To establish the application of liquid crystals as biosensors, the characterization of LC to detect protein is essential [14]. LC-Biomolecular analyte interaction gives rise to cell-signalling pathways [15,16], diagnostic assays for use in the low-resource environment [17] and potential drug discovery [18].

In 1998, N.L. Abbott initiated the use of LCs to study protein-binding [19,20], biomolecules [21,22] and ionic surfactants [23]. The interaction between liquid crystals and surfactant exhibit a significant change in the alignment of the LC molecules that can be used in detecting proteins [24]. The sensitivity of the LC-surfactant interaction with different biomolecules is reflected as textural changes used in biosensing. The silane properties of surfactant play a vital role in the alignment of the LCs by absorbing into the substrate based on the length of the alkyl chain [25]. Following Abbott's works, some other researchers have worked on liquid crystal based sensors on biomolecular analytes [26,27].

The challenges of sensing biomolecular binding events at the LC interfaces provided motivation for detecting human serum albumin using nematic liquid crystals. The liquid crystal 4′-pentyl-4-b iphenylcarbonitrile (5CB) is selected as it exhibits the nematic phase at room temperature. The potential of the LC to detect or sense the protein at a particular concentration is discussed in this work. This work emphasizes on a potential LC-based biosensor depending on the interactions between HSA and 5CB. The alignment induced on the surface of 5CB by the surfactant Dimethyl octadecyl [3-(trimethoxy silyl) propyl] ammonium chloride (DMOAP) is reported. The alignment tends to change from homeotropic to planar with the introduction of HSA at the LC-aqueous interface [22].

The interaction between nematic LC and biological species is a promising field as it does not require the use of label proteins such as fluorescence to detect the biomolecular events. Also, it does not require any complicated experimental setup, and thus this biosensor can be used in a low-resource environment. The changes in the alignment of molecules observed under polarising optical microscopy (POM) are presented in this paper. Protein-ligand molecular docking studies interactions help determine the binding locations, binding energies of the biomolecules like HSA with ligand 5CB liquid crystals. Temperature-dependent Raman spectroscopy investigated the vibrational properties to study the interactions caused by sensing of HSA by 5CB molecules are analysed and reported. This technique provides information about the inter and intramolecular [28] interactions and observed changes under the microscope as measurable quantities [29]. Raman studies on different liquid crystals [30-34], and amino acids [35,36] have already been undertaken. Hence, this strategy is expected to be a promising means to study the interactions of protein-liquid crystal binding events.

2. Methods

2.1. Materials

Dimethyl octadecyl [3-(trimethoxy silyl) propyl] ammonium chloride (DMOAP) and 4′-pentyl-4-biphenylcarbonitrile liquid crystal (5CB), were procured from Sigma Aldrich and used as received for various experiments. The nematic range attained by 5CB LC is 24 °C to 35 °C. The phase transition temperatures of pure 5CB and the textures under a polarising optical microscope (POM) were examined and found to agree with the literature [37,38]. Human serum albumin (HSA, A1653-5G) is purchased from Sigma Aldrich. Phosphate buffered saline (PBS) is prepared from 12.77 g/mol of Na_2HPO_4 and 3.16 g/mol of NaH_2PO_4 at pH 7.4. HSA free off fatty acids is prepared in the PBS. An extinction coefficient of 36,500 M^{-1} cm^{-1} at 280 nm is used to determine the protein concentration employing adsorption measurements. An aqueous solution of deionized (DI) water and ethanol (99% pure) were used to clean the microscopic glass slides.

2.2. Preparation of DMOAP coated glass slides

The surfactant DMOAP possesses a long alkyl chain. It absorbs into the surface and then induces homeotropic alignment of the LC molecules [39]. DMOAP solution was prepared by adding 1% (v/v) of DMOAP solution in 100 mL of DI water. The cleaned microscopic glass slides were baked for 15 min at 80 °C. After drying, 1% (v/v) DMOAP solution modified the surface. DI water was used to rinse off the excessive DMOAP solution from the slides. These coated slides were then dried under a stream of nitrogen gas.

2.3. Preparation of LC-protein cells

The cells were prepared by DMOAP modified slides placed at the bottom. These slides were attached with a mylar spacer of 12 μM and a non-reacting glue. The spacer was cut into the form of a square with an inlet on one side. LC is injected into the cell with the help of a syringe. Next, the target protein HSA of different concentrations (100, 300 and 600) μM were introduced into the cell, as shown in Fig. 1. At the LC interface, a strong bond between the LC and HSA was formed. Two varieties of cells were created. The LC filled cells without HSA were used as the control, whereas the LC filled cells with HSA were used to investigate the effect of protein-LC interaction.

3. Characterization techniques

3.1. Molecular docking

The computational study of the interaction between a receptor (protein) and a ligand (LC), was carried out with Blind Docking Server [40] available at http://bio-hpc.eu/software/blind-docking-server/. The structure of protein HSA was collected from Protein data bank (PDB) with PDB ID: 1AO6 and liquid crystal 5CB was obtained from ChemSpider in the extension of .mol file. The docked results were further analyzed with Discovery studio visualizer client 2020 from BIOVIA.

3.2. Polarizing optical microscopy

A Leica DM2700P, Germany polarizing optical microscope was used to study the textures of the LC-protein ensemble. The studies were conducted in two domains: variation with temperature and variation with concentration. The temperature-dependent studies

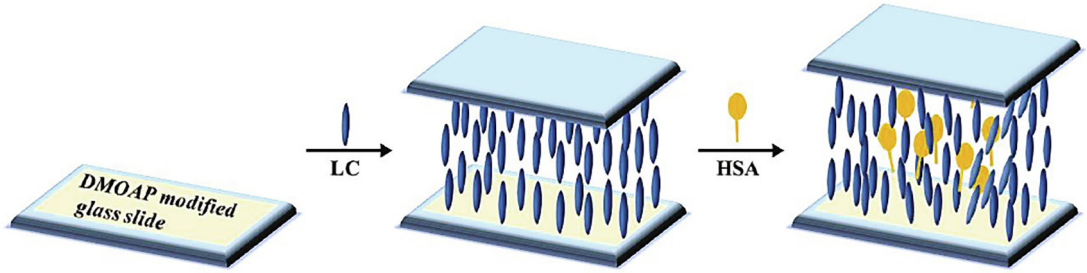

Fig. 1. Schematic presentation of the stepwise assembly of LC-protein cell.

were conducted in order to observe the changes that happened due to the orientational changes in LCs. These temperature-dependent studies were conducted for both the control cells and the HSA filled cells to eliminate the effects of the LCs. A Linkam hot stage LTS420, UK was mounted on the POM to accurately control and monitor the temperature. The POM was used with crossed polarizers in the transmission mode, and the images were captured by a Leica (MC170 HD) camera mounted on the microscope. The concentration-based studies were conducted to find the response, and at the same time, verify the textural changes due to the interaction of HSA with 5CB.

3.3. Raman spectroscopy

In this paper, the interaction of 5CB with proteins was further investigated by employing temperature-dependent Raman Spectroscopy with HSA 100 μM concentration. The particular concentration was considered by confirming the detection limit of LC to detect HSA, as obtained from the POM studies. The spectra were recorded with inVia Raman spectrometer from Renishaw, UK, equipped with 532 nm laser, and a charged coupled device detector. The sample was placed in a small well of 15 mm in diameter in a quartz sample holder. The holder was then mounted on a THM 600 Linkam hot-stage. The system was calibrated by recording the spectra at 520 cm^{-1} using silicon reference. Laser power was restricted to 5 mW to avoid laser heating of the sample. The sample was observed under a Leica DM 2500 M microscope attached with the instrument at a magnification of 50 × objective. The spectral parameters, namely, the peak position, the linewidth, and the integrated intensity, were measured accurately. The laser lines were recorded with a slit width of 50 μm maintained throughout the measurement. Each scan was repeated 50 times and averaged to obtain better results. The fitting of the curves and the deconvolution of various spectral parameters were achieved using the Thermocon GRAMS suite.

4. Results and discussions

4.1. Polarizing optical microscopy

The optical textures of pure 5CB on a DMOAP modified substrate in the nematic phase at 31 °C during the heating cycle in the range of 24–35 °C are shown in Fig. 2(a). The nematic phase shows a thread-like texture with line singularities. The isotropic phase of DMOAP-modified 5CB at 35 °C shows a completely dark background. On a molecular level, homeotropic alignment using DMOAP results from steric interactions between 5CB and DMOAP. Thus the surface density of DMOAP determines the quality of alignment [41]. This quality of alignment allows the ordering of the molecules in such a way that the textures in Fig. 2 become visible. Similar changes have also been reported where the increase of time and temperature vary the alignment, as eventually the sample flows uniformly and orient perpendicular to the surface [42]. During the heating and cooling of LC in the absence of HSA, we do not observe radial configuration in the surface. Fig. 2(c) shows the textural observation under POM between crossed polarizers just after adding HSA to the surface at room temperature.

The optical textures of the composite (5CB + HSA) are investigated under POM, as shown in Fig. 3. The isotropic point of DMOAP modified LC surface after exposure to HSA is 32.8 °C. The shift in the isotropic point of 5CB is due to the addition of HSA. Polarized optical images of DMOAP modified LC surface after exposure to the HSA for a minimum of 100 μM concentration is presented in Fig. 3(c). It shows the textures within a small temperature range from 30 °C to 32.5 °C. The initial texture is radial which transforms to twisted radial and then to bipolar before vanishing near the isotropic point. On cooling, the similar textures are not observed but a pre-radial texture forms on reaching 30.8 °C, where the direction of the radial changes from anticlockwise to the heating phase on clockwise in the configuration. The transition occurs mainly due to adsorption of HSA on LCs.

For concentrations of 300 and 600 μM, different configurations are observed from radial, pre-radial, twisted-radial and bipolar configurations but to varying positions at the interface. The pre-radial configuration seen in Fig. 3(a-c) has a single point defect. The bipolar configuration observed in Fig. 3(a-c) occurs either due to the hydrophobic interactions or π-π interactions among the molecules. These interactions occur among the phenyl groups of 5CB and the benzene rings of HSA residues. It is found that the 5CB droplets have a high charge density and helps to detect proteins. Also, to detect HSA, we have maintained the pH of the solution at a specific value of 4.2 as the charge state is dependent on the pH.

In Fig. 3, the droplets appear with different sizes, resulting in the difference of transition time for the director of molecules to change its configuration. The droplets smaller in size (Fig. 3 (b)) show the faster transfiguration of molecules in comparison to the larger droplets (Fig. 3 (a)). This method successfully detected HSA by LC with the help of POM under crossed polarizers. The sensing of HSA at a low concentration of 100 μM results in an effective sensing tool. The interaction with a low detection limit of HSA, short response time, and stability of LCs to detect HSA opens the way to use LC-based sensors.

4.2. Molecular docking

A molecular docking study is a computational program that predicts the most favourable position of the ligand when binding with the receptor to form a stable complex. The docking studies confirm the stability of LC docked with HSA. The lowest energy docked conformation of the cluster is selected and analysed. The structure of globular protein HSA is a heart-shaped having 585 amino acids, and 17 disulphide bonds [43,44]. It consists of two sites, namely

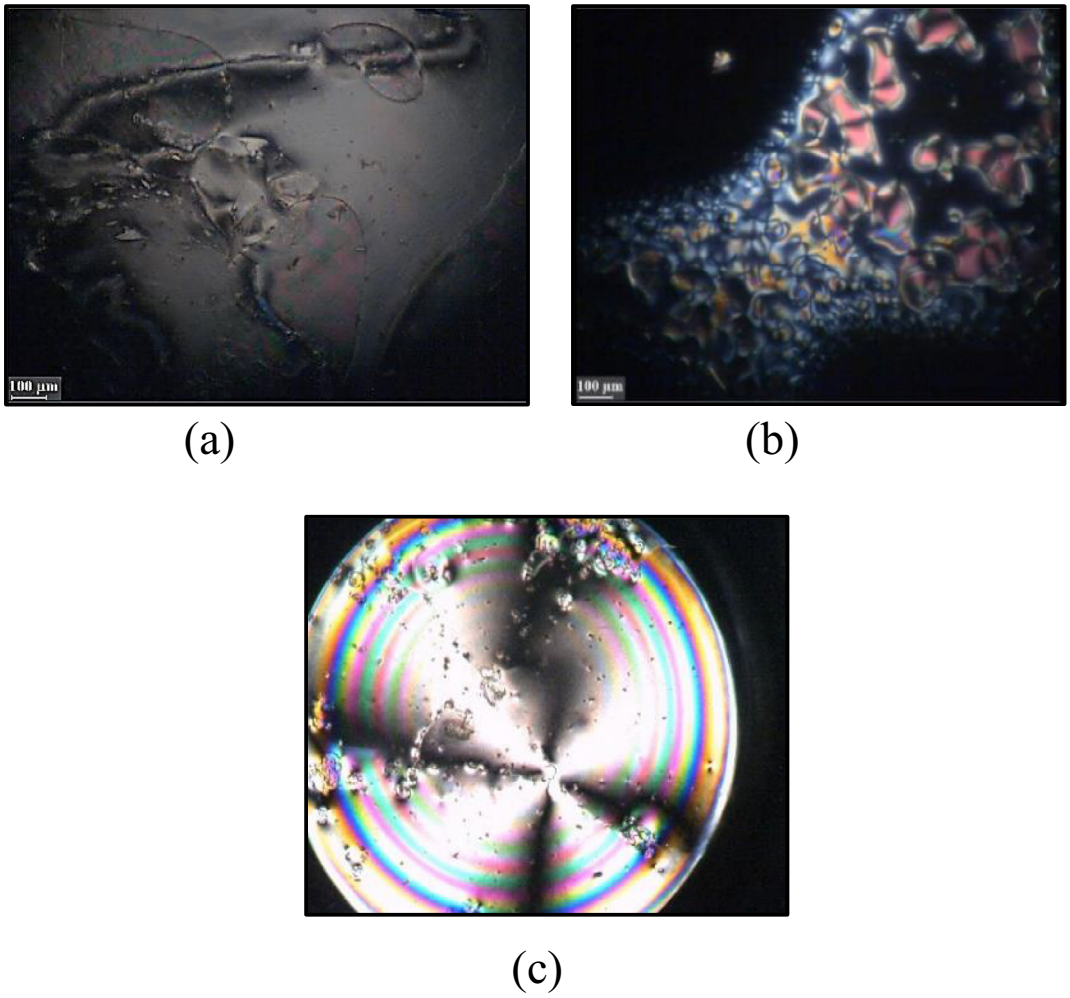

Fig. 2. Nematic phase during (a) heating and (b) cooling for DMOAP modified 5CB liquid crystal surface; (c) shows the optical image of the surface when HSA is added to the DMOAP modified LC surface.

Sudlow's site I (situated in subdomain IIA) and Site II (situated in subdomain IIIA) as shown in S.I. Fig. 1 [44]. These subdomains locate the binding site of the biomolecules. Based on the initial assessment of best binding poses, we observe that LC's most stable conformer to bind with HSA is Amide band I.

We found that the biphenyl rings of 5CB establish π-π interactions with PHE134, Tyr138, LYS137, LEU115, ARG186, LEU185, and Tyr161 present in the active sites of HSA to provide interacting regions. Amongst these, the benzene ring of PHE134 shows π-π stacking interactions with the 2nd phenyl ring of 5CB. LYS137 is found to stabilize 5CB with pi-alkyl interactions, as depicted in Fig. 4(a). LYS forms pi-alkyl interactions with the 2nd phenyl ring of 5CB. The benzene ring of both TYR 161, TYR138 interacts with the 1st phenyl ring of 5CB through π-π T-shaped interactions. TYR161,138 also shows pi-alkyl interactions with the 2nd carbon atom of 5CB. LEU185 and ARG 186 shows alkyl interactions with C-atom of 5CB. LEU115 interacts with pi-sigma bonds with 1st phenyl ring of 5CB. The bond distance is listed in Table 1. The solvent-accessible surface of 5CB is the cyano group, and that of HSA is in the residues. The bond distance of PHE to 5CB is 5.01 Å, TYR161 and TYR138 show bond distance of 5.29, 5.69, 5.0, and 5.04 Å concerning the phenyl ring and 2nd C-atom of 5CB, respectively. Leu115 shows the smallest bond distance of 3.89, Leu185 shows 4.83 Å, and Lys137 shows 4.21 Å bond distance. The region of ligand binding sites of HSA is located in subdomains IIA, and IIIA is corresponding to the site I and site II, respectively [45]. The Amide band I of the site I have the highest binding affinity, and the lowest binding energy is observed. Also, GLU141, LEU182, and ISOLEU142 stabilize the 5CB by forming Vander Waals interactions.

Fig. 4(a) represents the most stable conformer of the docked HSA at subdomain IB with the lowest binding energy of − 8.10 kcal. We select the docked poses as subdomain IB having the lowest binding energy and highest binding affinities. Fig. 4(b) and 4(c) display the receptor surfaces having hydrophobicity and H-bonds, respectively. The hydrophobicity region shows the docked poses of HSA-5CB inside the hydrophobic pockets along with the interacting residues at each binding sites.

The acceptor region is seen with the residues from PHE 134, where the oxygen bond readily accepts the hydrogen bond of the 5CB LC. Similarly, we can observe that the oxygen bond free in LYS 137, TYR 161, and TYR 138 acts as the binding surface's hydrogen bond acceptor. In contrast, the nitrogen atom in LYS 137 and the cyano group of 5CB acts as the hydrogen bond donor docked receptor surface. The white colour in Fig. 4(c) shows neither an acceptor nor a donor region.

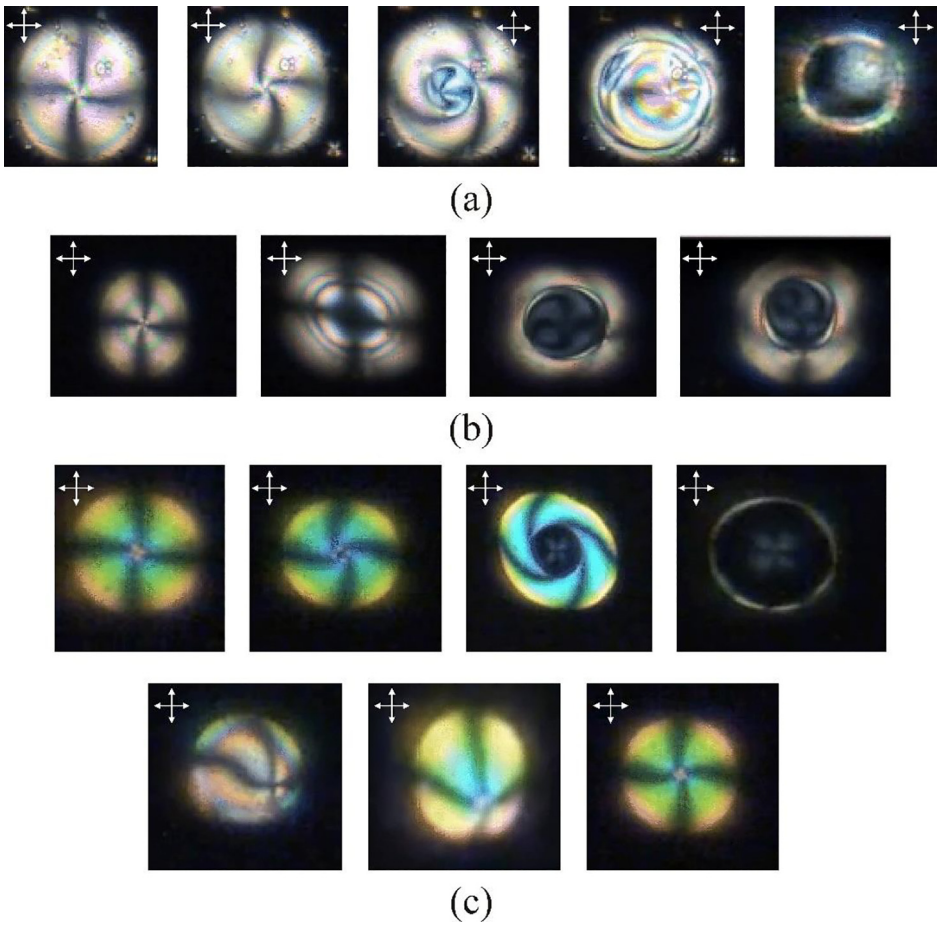

Fig. 3. Textures for 5CB-HSA at a concentration of a) HSA 300 μM b) HSA 600 μM c) HSA 100 μM.

4.3. Raman spectroscopy

Raman spectroscopy is a potential tool to study the vibrational properties of the interactions between LC and protein. Here, the technique is used to verify the interactions between 5CB-HSA observed from the POM and docking studies. For a better visibility, the spectral region 600–2400 cm^{-1} is divided into three parts viz. 600–900 cm^{-1}, 900–1400 cm^{-1} and 1400–2400 cm^{-1} as shown in Figs. 5–7. The variation in peak positions (PP), linewidth (LW) and integrated intensities (II) with temperatures ranging from −10 °C to 38 °C are discussed here. These parameters show the phase transitions of the samples and provide information on the structural change with the temperature. The PP, LW and II for 600–900 cm^{-1}, 900–1400 cm^{-1} and 1400–2400 cm^{-1} regions are summarized in S.I. Table 2.

4.3.1. Raman bands assignment in the region (600–900) cm^{-1}

In the region of 600–900 cm^{-1} presented in Fig. 5, the peak at 634 cm^{-1} at 38 °C increases to 636 cm^{-1} at 36 °C. At the isotropic point, i.e., 34 °C, it decreases to 634 cm^{-1}. As observed from the docking studies, the Tyrosine (TYR) residue of HSA binds with a phenyl ring of LC. The peak at 647 cm^{-1} is associated with TYR side chain, also reported in [35]. The presence of TYR in LC shows vibrations associated with the C-C stretching of the benzene ring, confirmed from the shift in peak position. The peak at 807 cm^{-1} and 826 cm^{-1} shows the presence of TYR, which then shifted to 809 cm^{-1} and 827 cm^{-1} respectively.

The band at 776 cm^{-1} is bending of CO_2^-,$\delta(CO_2^-)$ from Leucine. The peak 776 cm^{-1} at 38 °C gets shifted to 777 cm^{-1} at 36 °C, and the region of the temperature of LC, the peak gets shift to 775 cm^{-1}. The Tryptophan residue occurs at the band of 764 cm^{-1} which gets shifted due to the interaction of 5CB with HSA. A peak at 786 cm^{-1} is also observed at the temperatures of 32, 29, 26 and 23 °C. This peak disappears as the LC nematic phase, and the ordering is changed. The variations of LW, PP, and II of Raman bands in the region 600–900 cm^{-1} in Fig. 5 are shown in Fig. 8 and listed in S.I. Table 2.

The LW varying with temperature for Raman band 776 cm^{-1} are shown in Fig. 8(b). The LW changes with the temperature rise. A disturbance in the pattern could be visible with the increase of wavenumber. The reason is that during the transition from crystalline (K) to nematic (N), the bonds slowly starts breaking down with the decrease of energy. Subsequently, there is a shift in the PP and II, which is visible from Fig. 8(a) and 8(c), respectively. The II observes a decreasing trend in the bonds present with C-N stretch. This denotes the change in the alignment of the LC molecules. Due to the phenyl ring present in TYR, the surrounding single bonds show conformational changes with a charge transfer from electronegativity nitrogen to oxygen/carbon.

4.3.2. Raman bands assignment in the region (900–1400) cm^{-1}

The spectral region of 900–1400 cm^{-1} in Fig. 6 shows two to three peaks varying the temperatures. The Raman bands at 1177 cm^{-1} and 1183 cm^{-1} increase by 1 cm^{-1} and 2 cm^{-1} for low temperatures. Also, we observe that the peak at 1183 cm^{-1}

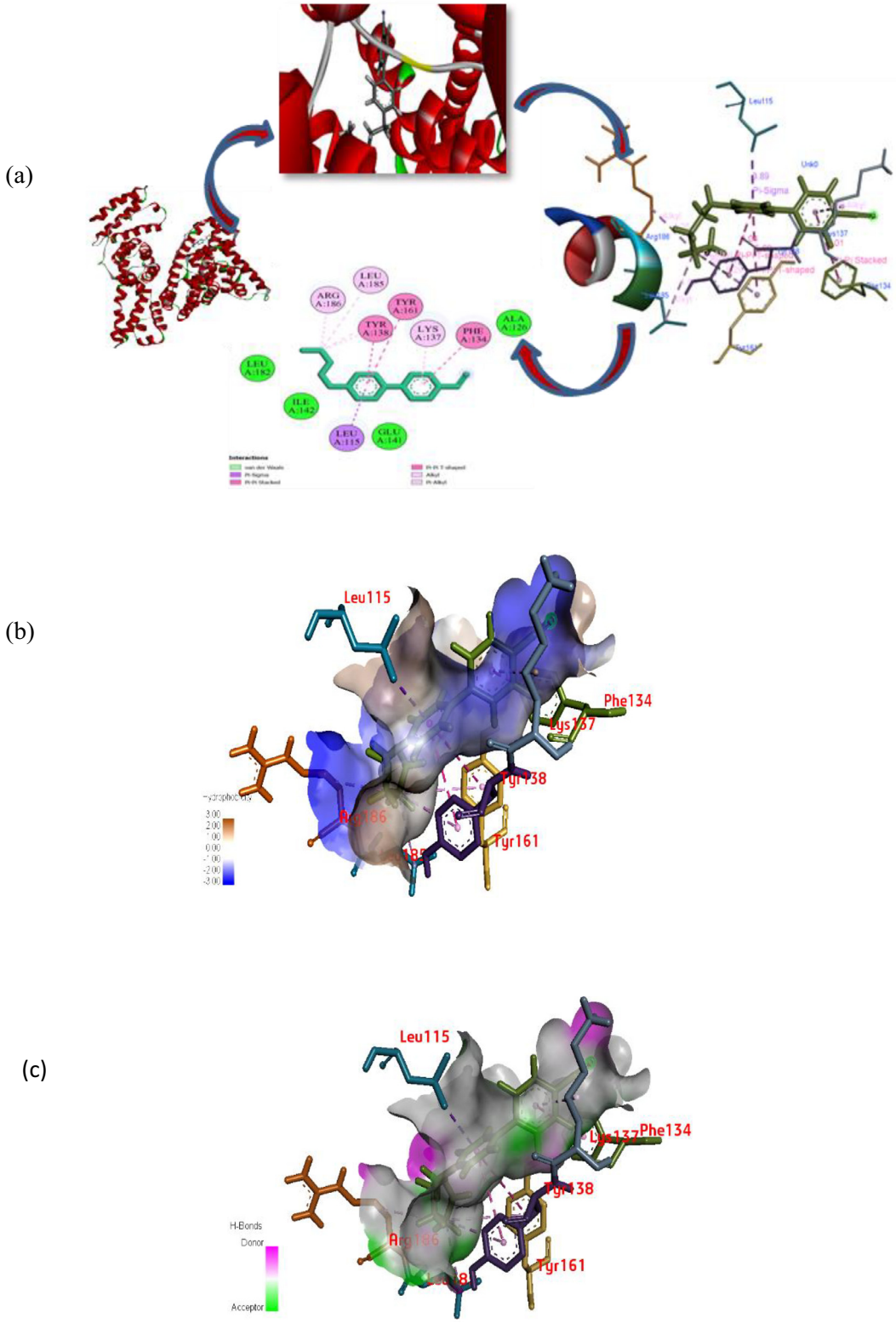

Fig. 4. Schematic presentation of (a) binding of LCs into protein; receptor surfaces showing (b) hydrophobicity (c) H-bonds.

vanishes at a temperature below 0 °C and is assigned in S.I. Table 1. The spectra result in the presence of TYR, which shows a peak at 1180 cm^{-1}.

The PP shows variable changes in the peaks with wavenumber during K-N phase transition observed in Fig. 9(a). The LW in Fig. 9(b) shows a sharp increase at temperature 25 °C at wavenumber 1183 cm^{-1} and gradually changes with the rise in wavenumber, as demonstrated in S.I. Table 2. The II shows a slight change during the N-I (isotropic) phase transition, as shown in Fig. 9(c).

Table 1
Detailed investigation about the residues involved in Protein-Ligand interaction.

Residue No.	Residue Type		Residue Chain	Distance (Å)
115	Leucine (LEU)		A	3.57
134	Phenylalanine (PHE)			3.65
137	Lysine (LYS)			3.52
137	Lysine (LYS)			3.75
138	Tyrosine (TYR)			3.56
141	Glutamic acid			3.71
161	Tyrosine (TYR)			3.75
182	Leucine (LEU)			3.75
185	Leucine (LEU)			3.90
186	Arginine (ARG)			3.73
Residue No.	**Residue Type**	**Residue Chain**	**Centre Distance (Å)**	**Angle (°)**
138	Tyrosine (TYR)	A	5.04	66.53
161	Tyrosine (TYR)		5.69	71.85

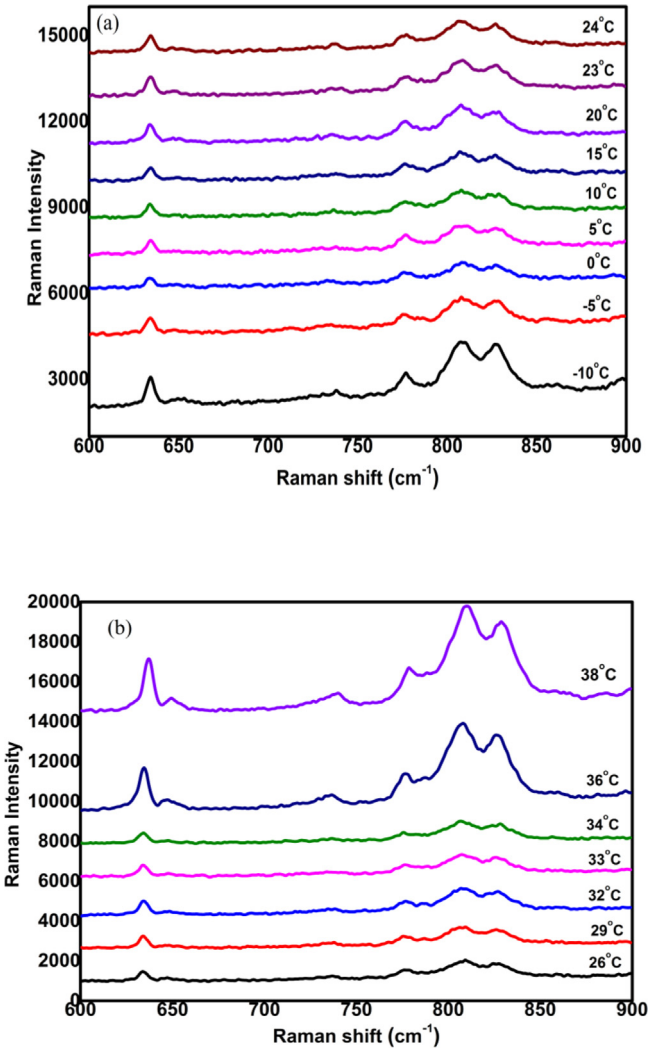

Fig. 5. Raman spectra for the region 600–900 cm^{-1}.

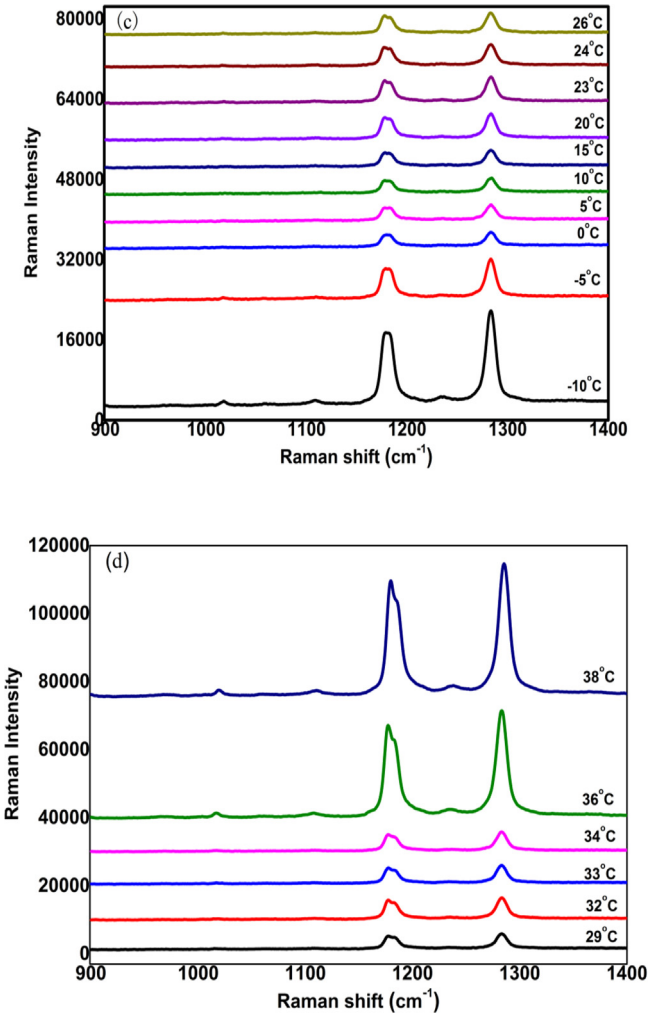

Fig. 6. Raman spectra for the region of 900–1400 cm-1.

4.3.3. Raman bands assignment in the region (1400–2400) cm^{-1}

Fig. 7 shows spectra at 1523 cm^{-1} with a band assigned in S.I. Table 1 which vanishes at a temperature of 33 °C and lower temperatures. We observe a peak at 1604 cm^{-1} which arises due to the benzene ring of 5CB. Also, a peak at 2224 cm^{-1} attributed to the cyano group, increases with a decrease in temperature. This peak indicates the presence of a cyano group attached to the end chain of 5CB LC. The PP, LW and II are presented in Fig. 10. The PP in Fig. 10(a) show changes with increasing wavenumber that indicate the changes or the independency of the molecules when it reaches the N-I phase transition. This decrease towards higher wavenumber describes a shift in the nematic phase. The LW shows

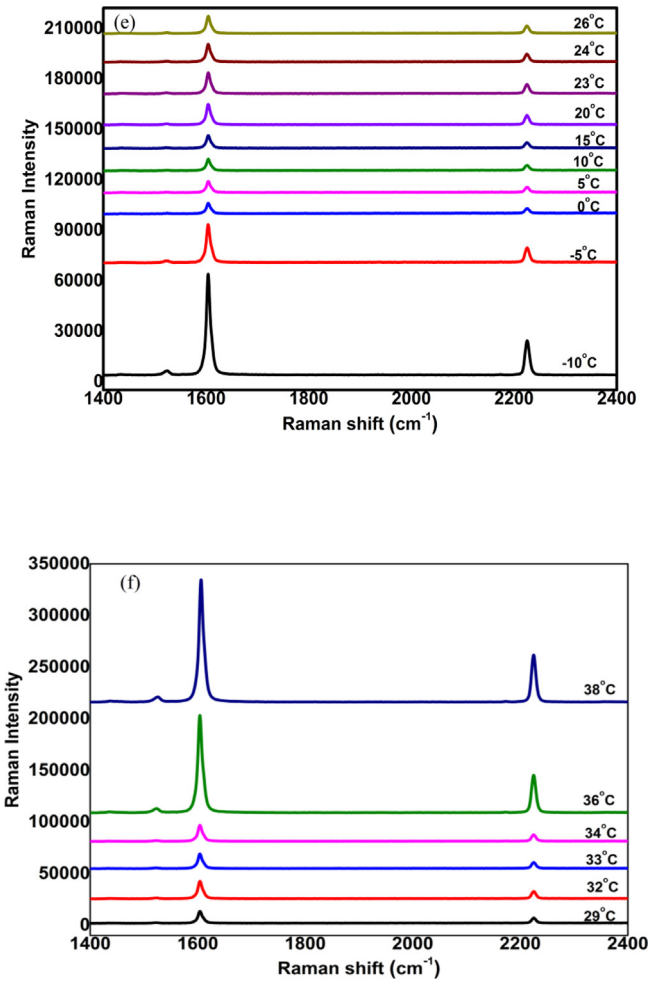

Fig. 7. Raman spectra for the region of 1400–2400 $cm^{-1.}$

a sharp increase with an increase in temperature depicted in Fig. 10(b). The II decreases with the rise of temperature in Fig. 10(c).

5. Conclusion

The interaction and detection of protein HSA with liquid crystal 5CB have been investigated using different techniques and molecular docking method. The POM studies confirm that the 5CB liquid crystal molecules change its orientation in the presence of foreign substance such as protein human serum albumin (HSA). It is efficient and straightforward to use 5CB as a transducing element for converting biological and chemical phenomenon into optical signals under a POM. Molecular docking studies were performed to support the experimental findings and determine the binding location of 5CB LC on HSA. This study reveals that the 5CB molecule binds with the subdomain IB with a binding energy of −8.10 kcal/-mol through hydrophobic and π-π interactions. The binding distances of the residues have been reported. The active sites have been confirmed with the experimental findings from Raman spectroscopy. The Raman studies acting as a sensing tool helped us to determine the vibrational properties of the interaction between 5CB LC and HSA. The temperature-dependent Raman spectra assign various functional groups present in the spectra during K-N and N-I transition. The studies have also been observed for low temperatures. The spectral changes result in an orientational disturbance of molecules and the inter and intramolecular interactions of molecules. The peak position, linewidth and integrated intensities with temperature variation are explored in the report. The parameters during phase transition show the breaking of the bonds due to low energy before reaching its isotropic point. The decrease in peak position towards higher wavenumber during N-I transition shows blue shifting in the spectra due to the transfer

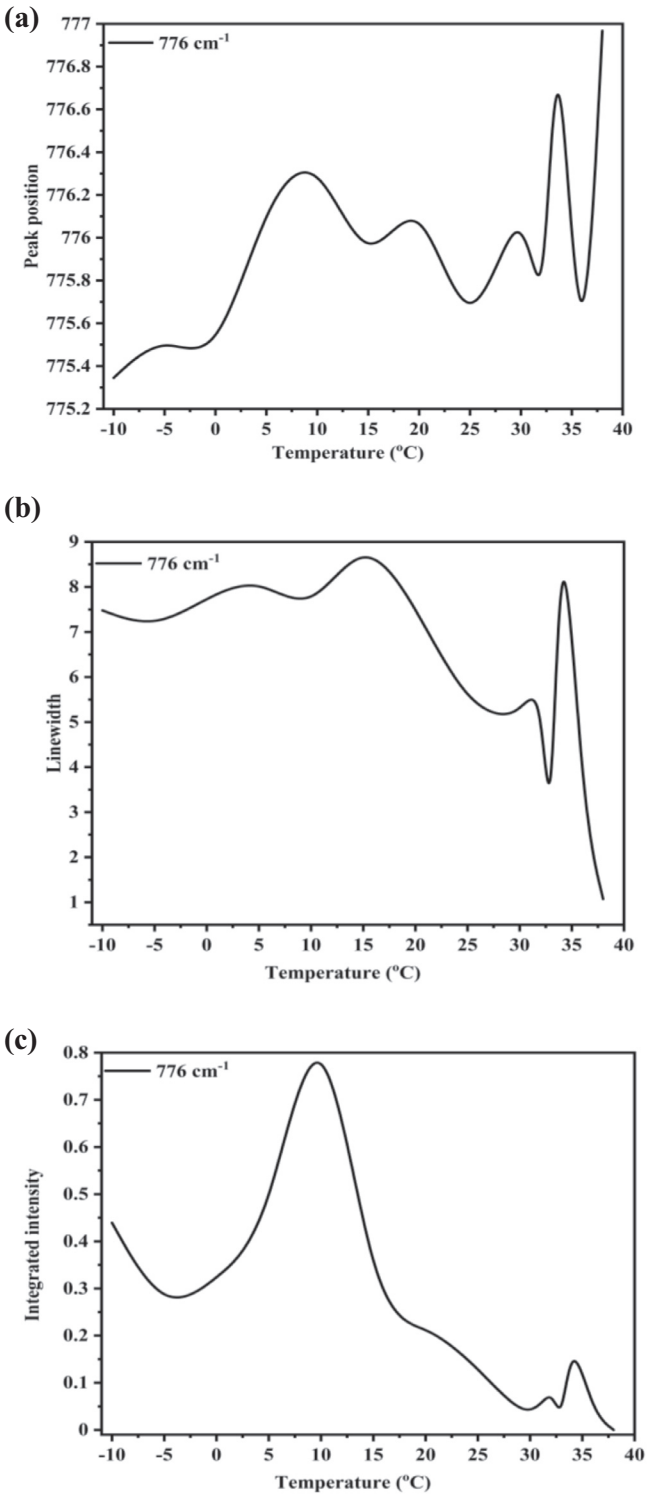

Fig. 8. Variation of peak position, linewidth and integrated intensity with temperature for 776 cm^{-1} of 5CB liquid crystals and human serum albumin.

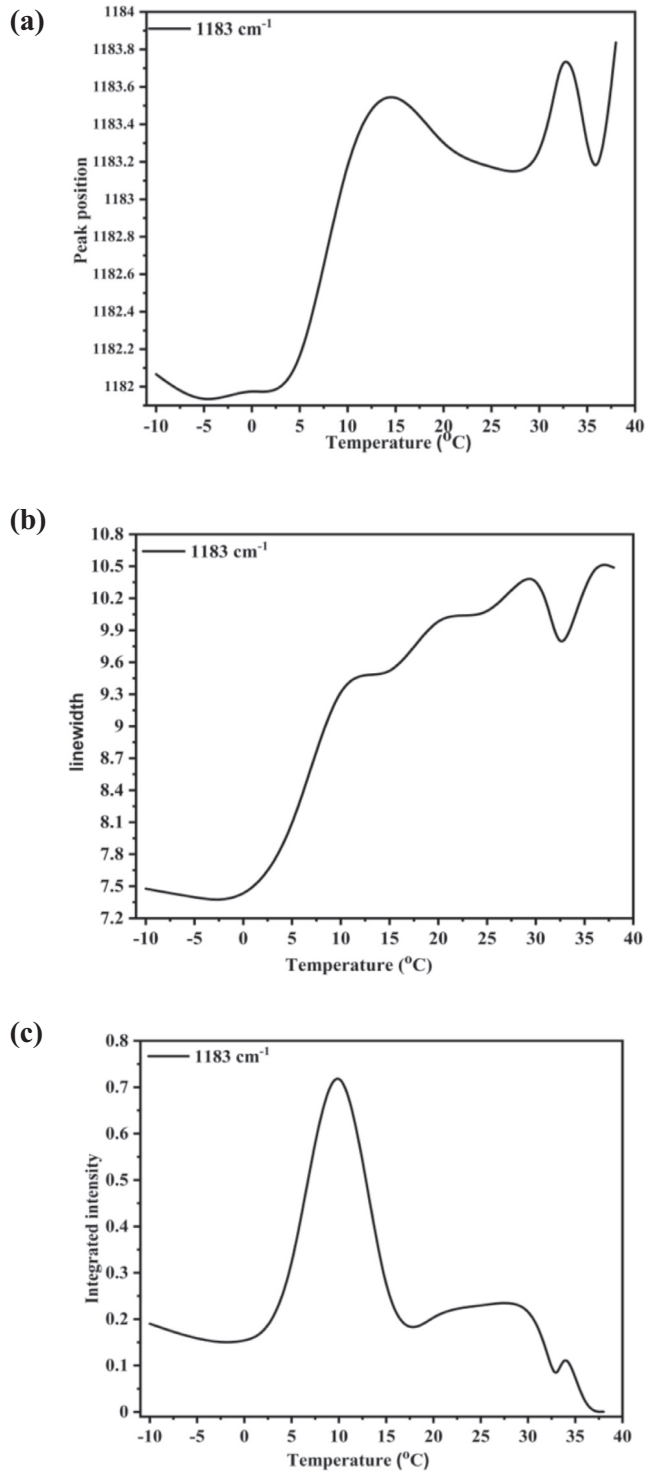

Fig. 9. Variation of peak position, linewidth and integrated intensity with temperature for 1183 cm^{-1} of 5CB liquid crystals and human serum albumin.

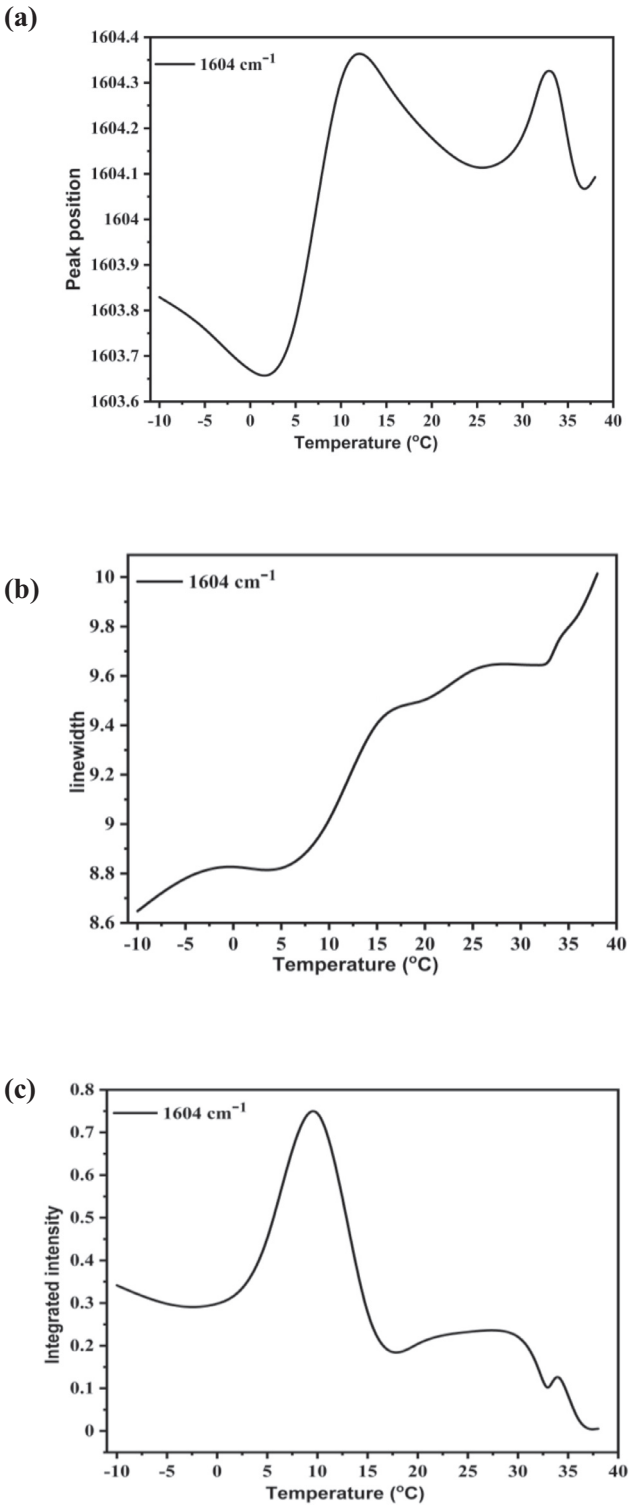

Fig. 10. Variation of peak position, linewidth and integrated intensity with temperature for 1604 cm^{-1} of 5CB liquid crystals and human serum albumin.

of charge density from one part to another chain of the molecule. It results in changes in the orientation of LC molecules in the presence of HSA. The findings provide information in spectral observation of the molecular interaction and vibrational changes caused by proteins in liquid crystals. Liquid crystals are potential materials for sensing as well as detecting applications without the use of complex instrumentation.

CRediT authorship contribution statement

Priyanki Kalita: Data curation, Formal analysis, Investigation, Visualization, Writing - original draft. **Shashank Sekhar Shukla:** Software. **Ranjan K. Singh:** Resources, Software. **Ayon Bhattacharjee:** Conceptualization, Data curation, Methodology, Project

administration, Resources, Software, Supervision, Validation, Writing - review & editing.

Declaration of Competing Interest

The authors declare that they have no known competing financial interests or personal relationships that could have appeared to influence the work reported in this paper.

Acknowledgement

The authors would like to thank the Department of Physics, Banaras Hindu University (BHU), Varanasi, UP for providing Raman spectroscopy characterization of the samples.

Appendix A. Supplementary data

Supplementary data to this article can be found online at https://doi.org/10.1016/j.saa.2021.119634.

References

[1] J.W. Kim, H. Kim, Lee Myoungbae, J.J. Magda, Interfacial tension of a nematic liquid crystal/water interface with homeotropic surface alignment, Langmuir 20 (2004) 8110–8113, https://doi.org/10.1021/la049843k.
[2] Fan F, Huang H, Wen S, Li T, Liu X, Wu Y, et al. Optical edge detection with adjustable resolution based on liquid crystal polarization gratings. Chinese Opt Lett Vol 18, Issue 9, Pp 093501- 2020;18:093501.
[3] P. Morawiak, M. Żurowska, W. Piecek, A long-pitch orthoconic antiferroelectric mixture modified by isomeric and racemic homostructural dopants, Liq Cryst 45 (2018) 1451–1459, https://doi.org/10.1080/02678292.2018.1446555.
[4] M.J. Lee, W. Lee, Liquid crystal-based capacitive, electro-optical and dielectric biosensors for protein quantitation, Liq Cryst (2019), https://doi.org/10.1080/02678292.2019.1673908.
[5] N. Ul Amin, H.M. Siddiqi, Y.K. Lin, Z. Hussain, N. Majeed, Bovine serum albumin protein-based liquid crystal biosensors for optical detection of toxic heavy metals in water, Sensors (Switzerland) 20 (2020), https://doi.org/10.3390/s20010298.
[6] Brake JM, Daschner MK, Luk Y-Y, Abbott NL. Biomolecular Interactions at Phospholipid-Decorated Surfaces of Liquid Crystals. Science (80-) 2003;302:2094–7. DOI:10.1126/science.1091749.
[7] S.L. Lai, W.L. Tan, K.L. Yang, Detection of DNA targets hybridized to solid surfaces using optical images of liquid crystals, ACS Appl Mater Interfaces 3 (2011) 3389–3395, https://doi.org/10.1021/am200571h.
[8] Z. Yang, J.K. Gupta, K. Kishimoto, Y. Shoji, T. Kato, N.L. Abbott, Design of Biomolecular Interfaces Using Liquid Crystals Containing Oligomeric Ethylene Glycol, Adv Funct Mater 20 (2010) 2098–2106, https://doi.org/10.1002/adfm.201000367.
[9] C.D. Ma, L. Adamiak, D.S. Miller, X. Wang, N.C. Gianneschi, N.L. Abbott, Liquid Crystal Interfaces Programmed with Enzyme-Responsive Polymers and Surfactants, Small 11 (2015) 5747–5751, https://doi.org/10.1002/smll.201502137.
[10] P. Popov, E.K. Mann, A. Jákli, Thermotropic liquid crystal films for biosensors and beyond, J. Mater. Chem. B 5 (2017) 5061–5078, https://doi.org/10.1039/C7TB00809K.
[11] Lin I-H, Miller DS, Bertics PJ, Murphy CJ, de Pablo JJ, Abbott NL. Endotoxin-Induced Structural Transformations in Liquid Crystalline Droplets. Science (80) 2011;332:1297–300. DOI:10.1126/science.1195639.
[12] Z. Hussain, F. Qazi, M.I. Ahmed, A. Usman, A. Riaz, A.D. Abbasi, Liquid crystals based sensing platform-technological aspects, Biosens. Bioelectron. 85 (2016) 110–127, https://doi.org/10.1016/j.bios.2016.04.069.
[13] D. Hartono, S.L. Lai, K.L. Yang, L.Y.L. Yung, A liquid crystal-based sensor for real-time and label-free identification of phospholipase-like toxins and their inhibitors, Biosens. Bioelectron. 24 (2009) 2289–2293, https://doi.org/10.1016/j.bios.2008.11.021.
[14] D. Zhao, Y. Peng, L. Xu, W. Zhou, Q. Wang, L. Guo, Liquid-Crystal Biosensor Based on Nickel-Nanosphere-Induced Homeotropic Alignment for the Amplified Detection of Thrombin, ACS Appl. Mater. Interfaces 7 (2015) 23418–23422, https://doi.org/10.1021/acsami.5b08924.
[15] R. Kopan, M.X.G. Ilagan, The Canonical Notch Signaling Pathway: Unfolding the Activation Mechanism, Cell 137 (2009) 216–233, https://doi.org/10.1016/j.cell.2009.03.045.
[16] J. Garcia Fortanet, C.H.T. Chen, Y.N.P. Chen, Z. Chen, Z. Deng, B. Firestone, et al., Allosteric Inhibition of SHP2: Identification of a Potent, Selective, and Orally Efficacious Phosphatase Inhibitor, J. Med. Chem. 59 (2016) 7773–7782, https://doi.org/10.1021/acs.jmedchem.6b00680.
[17] M. Funes-Huacca, A. Wu, E. Szepesvari, P. Rajendran, N. Kwan-Wong, A. Razgulin, et al., Portable self-contained cultures for phage and bacteria made of paper and tape, Lab Chip 12 (2012) 4269–4278, https://doi.org/10.1039/c2lc40391a.
[18] Jorgensen WL. The Many Roles of Computation in Drug Discovery. Science (80) 2004;303:1813–8. DOI:10.1126/science.1096361.
[19] Y.Y. Luk, M.L. Tingey, K.A. Dickson, R.T. Raines, N.L. Abbott, Imaging the binding ability of proteins immobilized on surfaces with different orientations by using liquid crystals, J. Am. Chem. Soc. 126 (2004) 9024–9032, https://doi.org/10.1021/ja0398565.
[20] Matthew L. Tingey, Sean Wilyana, Edward J. Snodgrass and, Abbott NL. Imaging of Affinity Microcontact Printed Proteins by Using Liquid Crystals 2004. DOI:10.1021/LA049728+.
[21] J.M. Brake, A.D. Mezera, N.L. Abbott, Active Control of the Anchoring of 4′-Pentyl-4-cyanobiphenyl (5CB) at an Aqueous-Liquid Crystal Interface by using a Redox-Active Ferrocenyl Surfactant, Langmuir 19 (2003) 8629–8637, https://doi.org/10.1021/la034469u.
[22] J.M. Brake, A.D. Mezera, N.L. Abbott, Effect of surfactant structure on the orientation of liquid crystals at aqueous-liquid crystal interfaces, Langmuir 19 (2003) 6436–6442, https://doi.org/10.1021/la034132s.
[23] I.H. Lin, M.V. Meli, N.L. Abbott, Ordering transitions in micrometer-thick films of nematic liquid crystals driven by self-assembly of ganglioside GM1, J. Colloid Interface Sci. 336 (2009) 90–99, https://doi.org/10.1016/j.jcis.2009.03.068.
[24] D. Wang, S.Y. Park, I.K. Kang, Liquid crystals: Emerging materials for use in real-time detection applications, J. Mater. Chem. C 3 (2015) 9038–9047, https://doi.org/10.1039/c5tc01321f.
[25] T. Nakagawa, M. Soga, Contact angle and atomic force microscopy study of reactions of n-alkyltrichlorosilanes with muscovite micas exposed to water vapor plasmas with various power densities, Japanese J. Appl. Physics, Part 1 Regul. Pap. Short Notes Rev. Pap. 36 (1997) 6915–6921, https://doi.org/10.1143/jjap.36.6915.
[26] S.H. Yoon, K.C. Gupta, J.S. Borah, S.Y. Park, Y.K. Kim, J.H. Lee, et al., Folate ligand anchored liquid crystal microdroplets emulsion for in vitro detection of KB cancer cells, Langmuir 30 (2014) 10668–10677, https://doi.org/10.1021/la502032k.
[27] M. Omer, S.Y. Park, Preparation of QP4VP-b-LCP liquid crystal block copolymer and its application as a biosensor, Anal. Bioanal. Chem. 406 (2014) 5369–5378, https://doi.org/10.1007/s00216-014-7900-y.
[28] S.K. Dash, R.K. Singh, P.R. Alapati, A.L. Verma, A comparative laser Raman study on TB4A, TB7A and TB10A, Liq Cryst 25 (1998) 459–465, https://doi.org/10.1080/026782998205967.
[29] B. Gogoi, A. Bhattacharjee, P.R. Alapati, A.L. Verma, Laser Raman studies on compounds 7.O4O.7 and 7.O5O.7, Liq. Cryst. 30 (2003) 931–938, https://doi.org/10.1080/0267829031000136066.
[30] N.M. Amer, Y.R. Shen, Raman scattering from nematic liquid-crystalline azoxybenzenes, J. Chem. Phys. 56 (1972) 2664–2667, https://doi.org/10.1063/1.1677593.
[31] B.J. Bulkin, F.T. Prochaska, Vibrational Spectra of Liquid Crystals. II. The Raman Spectrum of p -Azoxyanisole in Crystal, Nematic, and Isotropic Phases, 10–100-cm^{-1} Region, J. Chem. Phys. 54 (1971) 635–639, https://doi.org/10.1063/1.1674888.
[32] S.K. Dash, R.K. Singh, P.R. Alapati, A.L. Verma, Dynamics of phase transitions in a liquid crystalline compound (TBDA) probed by Raman spectroscopy, J. Phys. Condens Matter. 9 (1997) 7809–7815, https://doi.org/10.1088/0953-8984/9/37/012.
[33] S.K. Dash, R.K. Singh, B.P. Asthana, P.R. Alapati, A.L. Verma, A new phase transition in supercooled TBDA probed by low-temperature Raman study, J. Raman Spectrosc. 30 (1999) 81–84, https://doi.org/10.1002/(sici)1097-4555(199902)30:2<81::aid-jrs348>3.0.co;2-z.
[34] A. Bhattacharjee, P.R. Alapati, A.L. Verma, Dynamics of phase transitions in a liquid crystal probed by Raman spectroscopy, Liq. Cryst. 28 (2001) 1315–1320, https://doi.org/10.1080/02678290110038201.
[35] B. Sjöberg, S. Foley, B. Cardey, M. Enescu, An experimental and theoretical study of the amino acid side chain Raman bands in proteins, Spectrochim Acta - Part A Mol. Biomol. Spectrosc. 128 (2014) 300–311, https://doi.org/10.1016/j.saa.2014.02.080.
[36] M.C. Chen, R.C. Lord, Laser-Excited Raman Spectroscopy of Biomolecules. VIII. Conformational Study of Bovine Serum Albumin, J. Am. Chem. Soc. 98 (1976) 990–992, https://doi.org/10.1021/ja00420a021.
[37] N. Lebovka, V. Melnyk, Y. Mamunya, G. Klishevich, A. Goncharuk, N. Pivovarova, Low temperature phase transformations in 4-cyano-4'-pentylbiphenyl (5CB) filled by multiwalled carbon nanotubes, Physica E: Low-Dimensional Systems Nanostruct. 65–69 (2013) 52, https://doi.org/10.1016/j.physe.2013.03.029.
[38] T. Mansaré, R. Decressain, C. Gors, V.K. Dolganov, Phase transformations and dynamics of 4-cyano-4′-pentylbiphenyl (5CB) by nuclear magnetic resonance, analysis differential scanning calorimetry, and wideangle X-ray diffraction analysis, Mol Cryst Liq Cryst Sci Technol Sect A Mol Cryst Liq Cryst 382 (2002) 97–111, https://doi.org/10.1080/713738756.
[39] Y.K. Kim, K.R. Raghupathi, J.S. Pendery, P. Khomein, U. Sridhar, J.J. De Pablo, et al., Oligomers as Triggers for Responsive Liquid Crystals, Langmuir 34 (2018) 10092–10101, https://doi.org/10.1021/acs.langmuir.8b01944.

[40] I. Sánchez-Linares, H. Pérez-Sánchez, J.M. Cecilia, J.M. García, High-Throughput parallel blind Virtual Screening using BINDSURF, BMC Bioinformatics 13 (2012), https://doi.org/10.1186/1471-2105-13-S14-S13.
[41] K. Hiltrop, H. Stegemeyer, On the orientation of liquid crystals by monolayers of amphiphilic molecules, Berichte Der Bunsengesellschaft/Physical Chem. Chem. Phys. 85 (1981) 582–588, https://doi.org/10.1002/bbpc.19810850712.
[42] Dierking I. Textures of liquid crystals. Wiley-VCH; 2003 Verlag GmbH & Co. KGaA, Weinheim, Federal Republic of Germany (2003).
[43] S.A. Adcock, J.A. McCammon, Molecular dynamics: Survey of methods for simulating the activity of proteins, Chem Rev 106 (2006) 1589–1615, https://doi.org/10.1021/cr040426m.
[44] Peters J. Theodore, All About Albumin, Elsevier (1995), https://doi.org/10.1016/b978-0-12-552110-9.x5000-4.
[45] T.M.M. Abu, J. Ghithan, M.I. Abu-Taha, S.M. Darwish, M.M. Abu-hadid, Spectroscopic approach of the interaction study of ceftriaxone and human serum albumin, J. Biophys. Struct. Biol. 6 (2014) 1–12, https://doi.org/10.5897/jbsb2013.0045.